

Efficiency is doing things right: high-throughput, automated, 3D methods in the modern era of otolith morphometrics

Micah J. Quindazzi, Adam P. Summers, and Francis Juanes

Abstract: The morphometrics of fish otoliths have been commonly used to investigate population structures and the environmental impacts on ontogeny. These studies can require hundreds if not thousands of otoliths to be collected and processed. Processing these otoliths takes up valuable time, money, and resources that can be saved by automation. These structures also contain relevant information in three dimensions that is lost with 2D morphometric methods from photographic analysis. In this study, the otoliths of three populations of coho salmon (*Oncorhynchus kisutch*) were examined with manual 2D, automated 2D, and automated 3D otolith measurement methods. The automated 3D method was able to detect an 8% difference in average otolith density, while 2D methods could not. Due to the loss of information in the z axis, and the longer processing time, 2D methods can take up to 100 times longer to reach the same statistical power as automated 3D methods. Automated 3D methods are faster, can answer a wider range of questions, and allow fisheries scientists to automate rather monotonous tasks.

Résumé : La morphométrie des otolites de poissons a souvent été utilisée pour étudier les structures de populations et les impacts de l'environnement sur l'ontogénèse. Ces études peuvent nécessiter le prélèvement et le traitement de centaines, voire de milliers d'otolites. Le traitement de ces otolites prend du temps, de l'argent et des ressources précieuses que l'automatisation peut permettre d'épargner. Ces structures contiennent également de l'information tridimensionnelle intéressante que l'utilisation de méthodes morphométriques basées sur l'analyse de photographies évacue. Dans la présente étude, les otolites de trois populations de saumons cohos (*Oncorhynchus kisutch*) ont été examinés par des méthodes de mesure des otolites en 2D manuelle, en 2D automatisée et en 3D automatisée. Cette dernière méthode a pu détecter une différence de 8 % de la densité moyenne des otolites, ce que les méthodes 2D n'ont pu faire. En raison de la perte d'information le long de l'axe z et du temps de traitement plus long, les méthodes 2D peuvent prendre jusqu'à 100 fois plus longtemps pour atteindre la même efficacité statistique que des méthodes 3D automatisées. Ces dernières sont plus rapides, permettent de répondre à un plus grand éventail de questions et permettent aux spécialistes des sciences halieutiques d'automatiser des tâches plutôt monotones. [Traduit par la Rédaction]

Introduction

Morphometrics is the study of the variation of size and shape. While biologists have used morphometrics for centuries, the use of quantitative morphometrics of structures within organisms is more recent. The first wave of quantitative morphometrics was used for taxonomic and correlation studies (Thompson 1917; Phillips 1948). By the 1960s, multivariate analyses, such as principal components analysis (PCA), allowed for a second wave of quantitative morphometric studies that not only compared the correlation between two variables, but allowed for multiple correlations and covariations to be tested in one model (Sokal 1965). The third wave of quantitative morphometrics is known as geometric morphometrics; it uses outlines or landmarks to compare variation of forms across homologous points and to preserve the attributes of shape lost by prior methods (Adams et al. 2004). This era of quantitative morphometrics developed the use of 2D or 3D landmark points related to biologically significant regions of a structure to more accurately assess the differences in overall shape (Rohlf and Marcus 1993). Newer technologies, like high-resolution X-ray microcomputed tomography (HRXMT) and 3D Slicer, provide biologists with a new set of tools. These developments

have led to the possibility of high-throughput, automated, 3D morphometrics.

For many biological systems measuring all three dimensions is not important to capture the extent of morphological variation. If the specimen can be oriented so that there is minimal information contained in the z axis, then 2D analyses are perfectly adequate and can be automated with existing tools like ShapeR (Libungan and Pålsson 2015). Butterfly wings are a great example of a structure where a 2D analysis would likely capture the vast majority of the morphological variation. However, in many cases there is no orientation that sufficiently reduces the information in the third dimension, and so it becomes important to capture that geometric axis as an axis of variation. For example, when examining sculpin heads Buser et al. (2018) found that 2D and 3D morphospaces were quite different, with one clade diverging in the 2D but not the 3D analysis. They also found mouth size correlated with the importance of highly mobile prey items only when the z axis was included. Though a 3D analysis will cover more of the morphological variation over 2D analysis, 2D analysis is still commonly used because getting 3D data are both expensive and time consuming (Cardini 2014; Afanasyev et al. 2017). In recent years, methods to collect 3D information from samples have

Received 12 April 2021. Accepted 2 August 2021.

M.J. Quindazzi and F. Juanes. Department of Biology, University of Victoria, Victoria, BC V8P 5C2, Canada.

A.P. Summers. Department of Biology, University of Washington, Friday Harbor, WA 98250, USA.

Corresponding author: Micah J. Quindazzi (email: m.j.quindazzi@gmail.com).

© 2021 The Author(s). Permission for reuse (free in most cases) can be obtained from copyright.com.

become cheaper and easier to use, with techniques such as photogrammetry and computed tomography (CT). One method of getting 3D data from samples is HRXMT, which involves taking radiographs of samples at multiple angles to then produce a 3D volume. The 3D volume produced is accurate down to the scale of μm , though the newest models are accurate down to 200 nm (Hipsley et al. 2020). This method is also referred to more simply as microcomputed tomography (μCT). In the past 5 years μCT scanners have gotten cheaper; free, open source software has been developed; and new workflows are being documented to streamline the data collection process (Buser et al. 2020). Furthermore, new techniques for high-throughput μCT scanning decrease cost per specimen drastically especially since many materials can be reused in subsequent analyses (Hipsley et al. 2020).

Otoliths play a sensory role for the fish, and they serve many purposes for the ichthyologist. They are usually composed of aragonite (calcium carbonate) and organic material, and are nearly three times as dense as the body of fish; thus pressure waves can be detected by the fish as the otoliths move relative to the surrounding tissue (Degens et al. 1969; Popper and Lu 2000). The mineral and organic material form alternating bands in the form of daily rings or other periodic patterns tied to individual growth, and it is this feature that is often exploited by biologists (Pannella 1971; Geffen 1982). Mineral deposition can be impacted by many factors, including temperature, somatic growth, and genetics (Mosegaard et al. 1988; Conover 1990). This deposition causes differences in otolith microstructure that accumulate into differences in otolith macrostructure over time. Here we are not interested in chemical or microstructural differences in otoliths, but rather the emergent macrostructural differences that arise among different populations of fishes that can be detected through otolith morphometrics.

Otolith morphometrics have been used by fisheries scientists as a tool for body size determination, species determination, and stock discrimination within a species (Campana and Casselman 1993; Waessle et al. 2003). Generally, otolith morphometric studies have used simple linear analyses, such as otolith length (Waessle et al. 2003), or more complex 2D analyses, such as elliptical Fourier analysis and overall otolith shape (Campana and Casselman 1993; Tracey et al. 2006). Otolith differences correlate well with genetic differences, and therefore provide a cheap and robust method for studying stock discriminations within a species (Afanasyev et al. 2017). More recently, researchers have used 3D shape analyses to detect differences in the overall volume and density of otoliths, as well as the 3D contour of the otoliths (Bignami et al. 2013; Marti-Puig et al. 2016; Radford et al. 2021). While 2D analyses are generally useful for body size determination and stock discrimination, they will miss crucial details, such as changes in sulcus depth and morphology that would be identified in a 3D full shape analysis (Schulz-Mirbach et al. 2011). Traditional morphometric methods are also limited in terms of throughput; the researcher generally must analyze samples one at a time and pay special attention to orientation, photo quality, and extraneous factors that can impact the quality of the analysis. Automated 3D methods can be done in bulk, they will generally produce the same quality of image, and the researcher will have to pay less direct attention to the measurement process to get useable results. To alleviate the concerns over costs, fisheries managers do not even need to invest in the technology themselves, as there are plenty of facilities that can conduct bulk μCT scans for little to no cost outside of the shipment of samples. Essentially, automated 3D methods account for relevant z axis information contained within otoliths that are not accounted for by 2D methods, and in a fraction of the time without much direct involvement in the collection of the morphometric data by fisheries scientists.

The goals of this study were four-fold: (1) develop a technique for rapidly, quantitatively, μCT scanning hundreds of otoliths per hour; (2) use free, open source software to measure the dimensions and the density of the otoliths; (3) compare μCT scan-based dimensional measurements to microscopy based measurements both for accuracy and time spent per specimen; (4) determine whether there are population based differences in otolith dimensions and density.

Materials and methods

Sample collection

Sagittal otoliths (hereinafter “otoliths”) were collected from coho salmon (*Oncorhynchus kisutch*) from the Big Qualicum, Chilliwack, and Quinsam hatcheries (British Columbia, Canada). Coho salmon were selected from fish euthanized for multiple broodstock egg takes from 30 October until 19 December 2018. Since our collections were opportunistically collected from fish euthanized for the primary purpose of broodstock egg takes, no animal care approval was required for this study. For each coho salmon the sex, origin (hatchery or wild), and the fork length (FL) were recorded. Otolith pairs were removed, washed with deionized water, and cleaned of any excess organic material and moisture. They were then stored dry in pairs. Twelve aragonitic otolith pairs were selected for this analysis from each hatchery; six of the otolith pairs were from hatchery fish, and the other six were from wild fish. There was an equal distribution of males and females in each of these groups. One set of otoliths from the Chilliwack hatchery was removed due to a break in one of the otoliths before all the analyses could be completed.

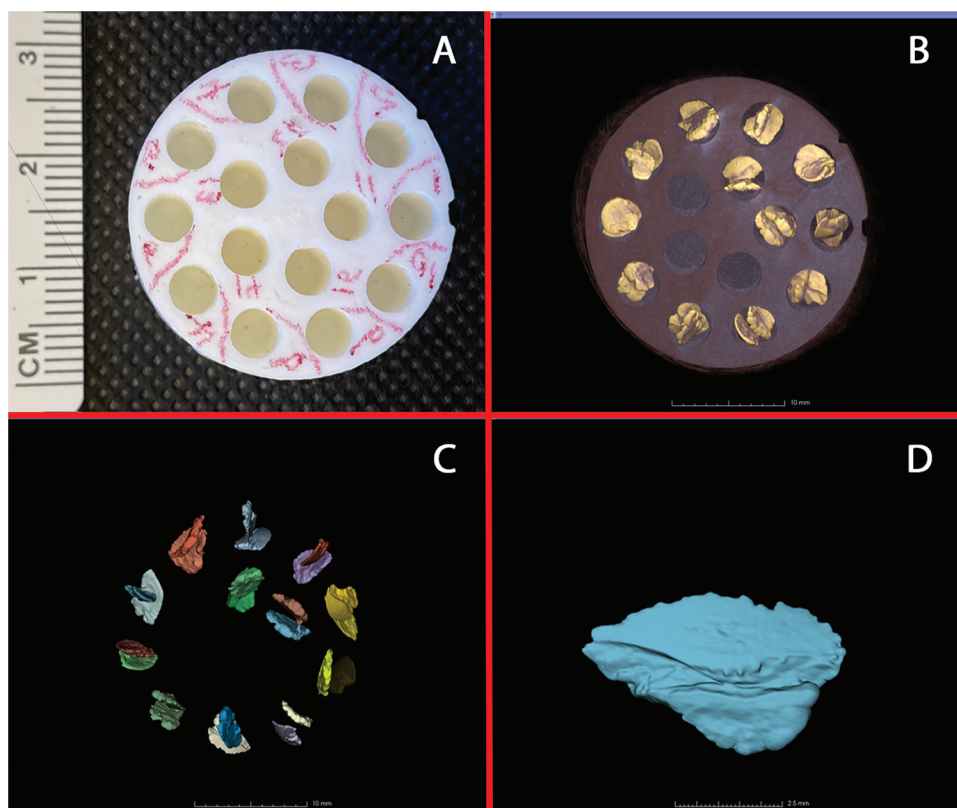
Otolith measurements

Otoliths were submerged in a plastic Petri dish filled with Super-Q deionized water. The distal side of the otoliths was viewed against a black background using an Olympus SZX16 stereoscope (Olympus, Shinjuku, Tokyo) at 20 \times magnification. Whole otolith photographs were captured by an Olympus DP26 camera (Olympus, Shinjuku, Tokyo) using the software Olympus cellSens Standard (Olympus, Shinjuku, Tokyo). Manual measurements of the Feret length (hereinafter called otolith length) and Feret width (hereinafter called otolith width) of the otoliths were collected by measuring the image within cellSens Standard to the nearest 5 μm . Measurements were replicated three times to examine variation among measurements. Otoliths were weighed with a Mettler Toledo ME104 analytical balance (Mettler Toledo, Columbus, Ohio) to the nearest 0.1 mg.

Photographs of the otoliths were then analyzed using the R package ShapeR. This R package automatically recorded the length, width, perimeter, and area of the otoliths to the nearest nanometer, but this was rounded to the nearest 5 μm as this was the resolution of the image. Average superficial density ($\text{g}\cdot\text{cm}^{-2}$) was calculated for each coho salmon by dividing the combined weight by the total surface area of both otoliths. While ShapeR is generally used to investigate overall 2D shape differences between stocks using elliptical Fourier analysis, this was not examined within this study.

Three sample holders were 3D printed with an Ultimaker S5 (Ultimaker, the Netherlands) using Ultimaker Tough PLA (Ultimaker, the Netherlands; Fig. 1A). Each holder was a plastic cylinder that had 24 wells spaced out equidistantly from one another, into which the otolith pair from one fish was placed (Fig. 1B). The three holders were attached to each other by winding thin plastic packing film around them. The stack of three holders were μCT -scanned with a Bruker SkyScan 1173 microsource CT (μCT) scanner (MicroPhotonics, Allentown, Pennsylvania) with a 1 mm aluminum filter at 60 μA and 133 mV. The resolution of the CT scan was 13.8 μm . The projections were processed into slice data with the Bruker proprietary software nRecon (Bruker, Germany), then visualized

Fig. 1. (A) One of the three sample holders that were 3D printed with an Ultimaker S5 (Ultimaker, the Netherlands) using Ultimaker Tough PLA (Ultimaker, the Netherlands). 15 wells existed in each holder. (B) Otolith holder with 24 coho otoliths as viewed when CT-scanned. One pair of otoliths per fish was put in each individual well. Scale bar indicates 10 mm. (C) Otoliths segmented into individual otoliths using the “Islands” function in 3D Slicer (www.slicer.org). Scale bar indicates 10 mm. (D) View of the sulcus side of one of the coho otoliths. Scale bar indicates 2.5 mm. [Colour online.]



and analyzed with the free, open-source software 3D Slicer (www.slicer.org). Otoliths are the only material in the CT scan with a significant density, far above the plastic sample holder or the background air. Due to this substantial difference in density, the automatic threshold detection algorithm within 3D Slicer will set an appropriate threshold based around the density of the otoliths. Setting a manual threshold is possible, but this likely would not impact the results of this study. First, a bounding box is created using the automatic threshold with all of the samples contained within it. Next, under the “Island” function we can split islands into segments (Fig. 1C). This entails splitting every disconnected, radio-dense, 3D volume into its own segment (Fig. 1D). 3D Slicer can then calculate the volume, diameters in all three dimensions (length, width, thickness), mass, average density, centroid, and xyz extents by using the “SegmentStatistics” tool. The length measured is also the Feret length, but width is measured as the longest distance between two tangential lines perpendicular to the Feret length, and thickness is the shortest distance between two tangential lines perpendicular to the Feret length.

Average otolith density was determined from μ CT scans by dividing the combined volume of both otoliths by the combined mass. Since all of the otoliths were scanned at the same time with constant settings, the densities are comparable among these data. Otolith μ CT scanning was conducted at the Friday Harbor labs (Washington, USA). Otolith scans and the resulting segmentations are available on OpenScience Framework.

Average otolith morphometrics, rather than left and right otolith morphometrics, were used for this study as individual coho salmon were used as the unit of replication.

Data analysis

Data were analyzed with R-studio (RStudio Team 2015; R Core Team 2020). Linear regression models were generated for comparisons between the different types of morphometric measurements estimated by each method. Analyses of variance (ANOVA) was used to determine the impacts of hatchery, sex, origin (hatchery stock or wild stock), and the interactions between these factors, on the otolith morphometrics of each coho salmon. Nonsignificant interactions were removed from models, and nonsignificant factors were combined. Models reported in this study were plotted through the “ggplot2” package (Wickham 2016).

Power analyses were conducted to compare the models of hatchery vs. otolith superficial density ($\text{g}\cdot\text{cm}^{-2}$) and hatchery vs. otolith density ($\text{g}\cdot\text{cm}^{-3}$). A power curve simulation was run using the R package *simr* (Green and MacLeod 2016) to estimate how many samples would be needed to achieve the same statistical power across both methods (keeping power and alpha constant). Power was set at 80% and alpha was set at 0.05. We ran 1000 power curve simulations for both datasets. To reach the parameters indicated for superficial density, we extended the model by 150 samples. We also qualitatively compared the time usage across methods.

Results

Samples

Coho salmon ranged in FL from 52.8 to 82 cm. Average coho salmon FLs were different among hatcheries ($F_{[2,32]} = 4.342$, $p = 0.022$) and a post hoc Tukey’s test revealed this was driven by a

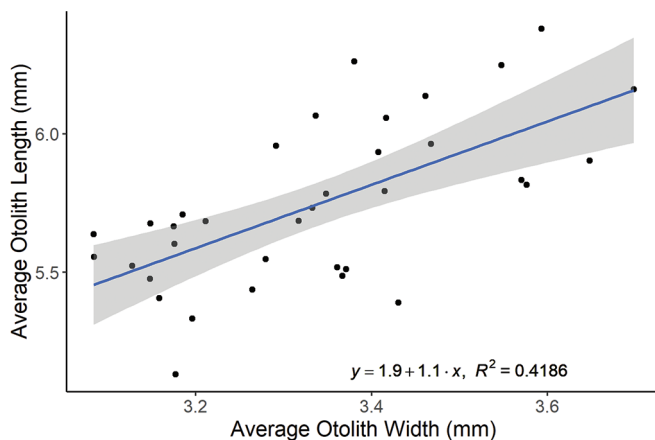
Table 1. Ranges and averages (in parentheses) of various otolith morphometric relationships from the three hatcheries in this study.

Hatchery	Length (mm) ^a	Width (mm) ^a	Perimeter (mm) ^a	Area (mm ²) ^a	Superficial density (g·cm ⁻²) ^a	Total volume (cm ³) ^b	Density (g·cm ⁻³) ^b
Big Qualicum	5.41–6.26 (5.76)	3.15–3.57 (3.33)	14.2–16.0 (15.1)	11.6–14.1 (12.8)	0.100–0.127 (0.109)	$0.960 \times 10^{-2} - 1.43 \times 10^{-2}$ (1.10×10^{-2})	2.11–2.69 (2.52)
Chilliwack	5.39–6.13 (5.72)	3.08–3.65 (3.32)	14.0–16.0 (15.0)	11.5–14.1 (12.7)	0.102–0.120 (0.109)	$0.971 \times 10^{-2} - 1.25 \times 10^{-2}$ (1.11×10^{-2})	2.45–2.61 (2.50)
Quinsam	5.13–6.38 (5.75)	3.08–3.70 (3.35)	13.8–16.6 (15.1)	10.9–15.2 (13.0)	0.103–0.123 (0.111)	$0.847 \times 10^{-2} - 1.36 \times 10^{-2}$ (1.06×10^{-2})	2.70–2.76 (2.73)

Note: With the exception of otolith volume, the following are the average values of the left and right otoliths. Volume is presented here as the total volume. All values have been rounded to three significant figures. Sample sizes for each hatchery are 12 for Big Qualicum, 11 for Chilliwack, and 12 for Quinsam.

^aValues drawn from ShapeR dataset.

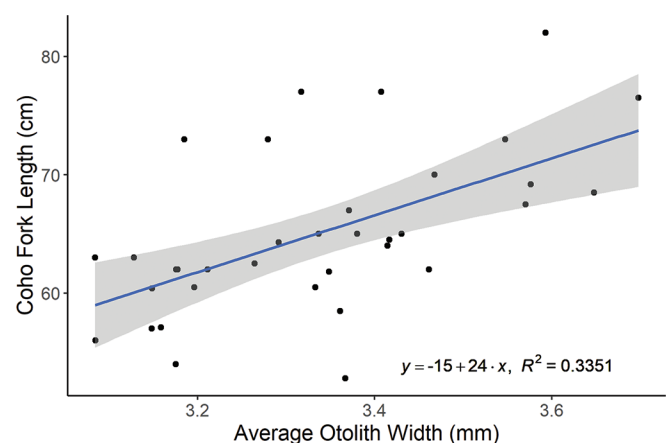
^bValues from microCT scan dataset.

Fig. 2. Linear relationship between the average otolith length and width of coho salmon from the Big Qualicum, Chilliwack, and Quinsam hatcheries from the year 2018 ($n = 35$). The line represents a linear regression line, with the grey area indicating standard error.

difference between the Quinsam and Chilliwack fish, with Quinsam coho being 7.5 cm larger on average. The differences in average FL among hatcheries was accounted for in all further analyses. If FL was not a significant term within the model, it was dropped from the model. On average, male coho were 4.8 cm longer than female coho. However, the sex of the coho itself had no significant impact on any aspect of otolith shape or size. The origin of the coho, i.e., whether they were hatchery or wild, had no discernable impact on the average FL ($t_{[33]} = 1.188$, $p = 0.243$). Sex and origin were included in the initial steps of the following models, but they were nonsignificant in every model so they were dropped from the final models reported on in this study.

Otolith measurements

Thirty-five coho otolith pairs were measured in total: 11 from the Chilliwack hatchery, and 12 each from the Big Qualicum and Quinsam hatcheries (Table 1). The manual measurements of the otoliths showed some variation between measurements, with the standard error (SE) of length measurements being 5.97 μm and the SE of width measurements 12.7 μm . When accounting for FL, otolith length and width did not differ across the hatcheries ($F_{\text{length } [2,31]} = 0.11$, $p_{\text{length}} = 0.896$; $F_{\text{width } [2,31]} = 0.173$, $p_{\text{width}} = 0.842$), and both metrics were closely related to each other ($R_{\text{adj}}^2 = 0.419$, $p < 0.001$; Fig. 2). Average otolith length and width were correlated with coho salmon FL ($R_{\text{adj}}^2 = 0.298$, $p < 0.001$; $R_{\text{adj}}^2 = 0.335$, $p < 0.001$), with width having a slightly stronger relationship (Fig. 3). When accounting for FL, otolith mass was not significantly different across hatcheries ($F_{[2,31]} = 0.910$, $p = 0.413$), or origin ($t_{[33]} = 0.268$, $p = 0.790$), and while there was no directional asymmetry, on average the otoliths pairs differed in mass by 3.4%. Otolith mass asymmetry was not different across hatcheries ($F_{[2,32]} = 0.960$, $p = 0.394$) or origin ($t_{[33]} = -0.758$, $p = 0.454$).

Fig. 3. Linear relationship between the coho salmon fork length (FL) and average otolith width of coho salmon from the Big Qualicum, Chilliwack, and Quinsam hatcheries from the year 2018 ($n = 35$). The line represents a linear regression line, with the grey area indicating standard error.

The average manual otolith length and width measurements were nearly identical to the length and width measurements produced automatically by ShapeR ($R_{\text{adj}}^2 > 0.999$, $p < 0.001$ for all length width measurements). ShapeR will produce the same values as long as the image and settings are the same. Along with the otolith length and width, ShapeR also provided values for the otolith perimeter and area. When accounting for FL, otolith perimeter and area did not vary across hatcheries ($F_{\text{perimeter } [2,31]} = 0.150$, $p_{\text{perimeter}} = 0.861$; $F_{\text{area } [2,31]} = 0.563$, $p_{\text{area}} = 0.575$) or origin ($t_{\text{perimeter } [33]} = 0.249$, $p_{\text{perimeter}} = 0.805$; $t_{\text{area } [33]} = 0.022$, $p_{\text{area}} = 0.983$). Otolith area provided a stronger relationship with coho salmon FL than either length or width ($R_{\text{adj}}^2 = 0.418$, $p < 0.001$). The superficial otolith density was not significantly different among hatcheries ($F_{[2,32]} = 0.476$, $p = 0.626$), although it was highest overall in the Quinsam hatchery (Fig. 4).

The μCT scanner added volumetric and density data along with all other morphometric values measured previously ($R_{\text{adj}}^2 > 0.999$, $p < 0.001$ for all four measurements). Measurements produced by the μCT scanner will have no variation as long as the same image and settings are used. We note that non-CT based measures of volume are quite difficult to do on otoliths that are this small. There was one density measurement from the Chilliwack hatchery that appeared as an outlier, with CH18-225 having an average otolith density of 2.105 $\text{g}\cdot\text{cm}^{-3}$. This observed density was far outside reported values for aragonite and may be a potential outlier. We report results of the 3D data with and without the potential outlier. When accounting for FL, otolith volume was not significantly different across hatcheries ($F_{[2,31]} = 0.726$, $p = 0.492$ with potential outlier; $F_{[2,30]} = 0.537$, $p = 0.590$ without potential outlier). Otolith density was significantly different across hatcheries ($F_{[2,32]} = 26.31$, $p < 0.001$ with potential outlier; $F_{[2,31]} = 67.73$,

Fig. 4. Boxplots showing the average otolith superficial density of coho salmon from the Big Qualicum (BQ; $n = 12$), Chilliwack (CH; $n = 11$) and Quinsam (Q; $n = 12$) hatcheries. Outliers are indicated by black dots. No significant differences were detected across hatcheries (see text for details). [Colour online.]

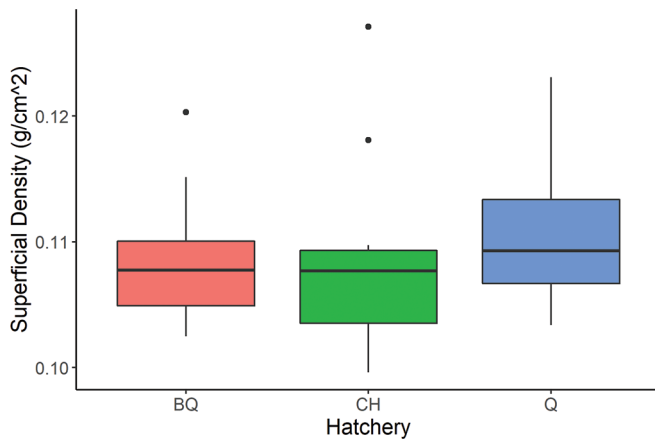
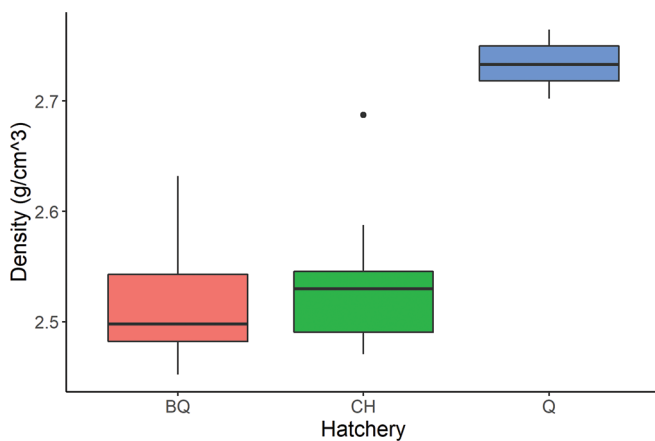


Fig. 5. Boxplots showing the average otolith density of coho salmon from the Big Qualicum (BQ; $n = 12$), Chilliwack (CH; $n = 10$) and Quinsam (Q; $n = 12$) hatcheries. CH18-225 is not included in this figure, as it was identified as a potential outlier. Significant differences were detected across hatcheries (see text for details). [Colour online.]



$p < 0.001$ without potential outlier), with Quinsam having the densest otoliths at $2.735 \text{ g}\cdot\text{cm}^{-3}$ on average (Fig. 5). The mass measured by the μCT scanner was significantly correlated to weights collected by hand ($R_{\text{adj}}^2 > 0.999$, $p < 0.001$).

The difference in strength between the 2D and 3D analyses was investigated by comparing the statistical power of superficial density and real density analyses. The superficial density data were extended by 150 otolith pairs per hatchery to reach a power of 80%, as the power of the initial analysis based on 11–12 pairs per hatchery was only 12.6%. Regardless of whether or not CH18-225 was included, the 2D superficial density metric reached 80% power at around ~110–130 otolith pairs per hatchery (Fig. 6), while the 3D density metric reached the same alpha and power values at around 3–4 otolith pairs per hatchery (Fig. 7).

Time usage

Time usage was not strictly quantified in this analysis, but rather approximations are provided based on experience. Otolith photography can vary between 1–5 min per otolith depending on

Fig. 6. Power curve simulation of ANOVA of superficial otolith density ($\text{g}\cdot\text{cm}^{-2}$) of fish from the Big Qualicum, Chilliwack, and Quinsam hatcheries based upon the data of the 35 otolith pairs in this study. Observations were extended to 150 otolith pairs per hatchery. Power was set at 80% and alpha was set at 0.05. These conditions were met between 110–130 coho salmon per hatchery.

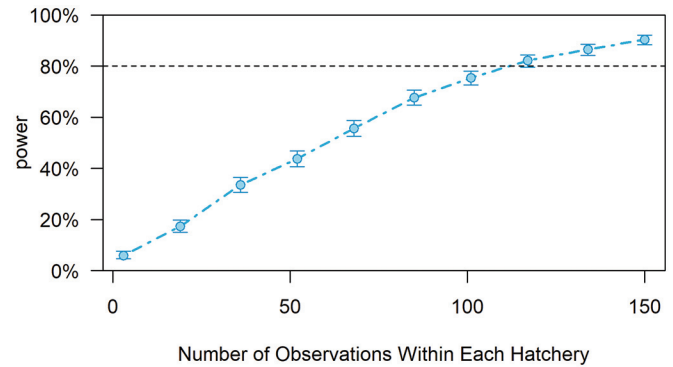
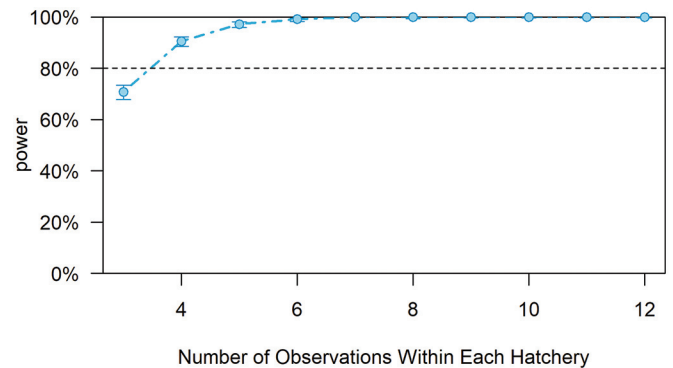


Fig. 7. Power curve simulation of ANOVA of otolith density ($\text{g}\cdot\text{cm}^{-3}$) of fish from the Big Qualicum, Chilliwack, and Quinsam hatcheries based upon the data of the 35 otolith pairs in this study. Power was set at 80% and alpha was set at 0.05. These conditions were met between 3–4 coho salmon per hatchery.



the condition of the otoliths being examined. Otoliths must be correctly oriented with all extraneous organic particles removed. The otolith length and width can be manually measured within 1 min per otolith depending on how the photo was taken and how easy it is to discern the correct measurement axes. ShapeR takes roughly 1 min to produce the otolith length, width, perimeter, area, and the shape file for an otolith. ShapeR also fails to recognize the outline of the otolith roughly 10% of the time (8 in the initial run during this study), resulting in further time spent on editing the photo or settings to produce an accurate outline. On average, it takes 3 min to conduct either a manual measurement or a 2D automatic measurement. In contrast, all 70 otoliths were μCT scanned in 45 min, resulting in an otolith being completed every ~40 seconds. On average, 4.5 otoliths are imaged and measured by the μCT scanner for every otolith analyzed by hand or with ShapeR.

Discussion

When measuring otoliths by hand, there are a few problems to overcome. Observers need to distinguish the Feret measurement axes to measure correctly, there is inherent measurement error, and it can be time consuming. Here we can see that an experienced researcher can generally keep repeatability rates to about the limit of detection, but for less skilled observers there is

greater room for error. Conducting a study with many otoliths is a monotonous task that can result in errors. And yet, with all of these problems, only a limited amount of information can be collected. In this study, otolith length and width were correlated with the fork length of the coho but and these relationships did not differ between stocks. This of course is not surprising for anyone who has worked with otolith morphometrics, as sample sizes tend to need to be in the hundreds, if not thousands (Campana and Casselman 1993; Waessle et al. 2003; Hüsey et al. 2016). To increase the amount of information collected by hand, it is possible to use software such as ImageJ (National Institutes of Health, Bethesda, Maryland) to measure the otolith perimeter and area. However, conducting otolith morphometrics manually is inefficient given the technology available to fisheries scientists today.

Automated 2D measurements of otolith length, width, perimeter, and area can be captured by ShapeR in about a fifth of the time it would take an experienced observer to produce them without nearly as many issues with repeatability or reproducibility. ShapeR can be run in the background allowing researchers to focus on other tasks. Another advantage of ShapeR over manual measurements is the automatic production of Fourier and Wavelet coefficients to distinguish species and populations within a species. This method has proved to be a useful tool for fisheries scientists investigating differences between stocks (Libungan and Pálsson 2015; Song et al. 2019). We were not surprised to find that with our 2D morphometric data, we were unable to find differences among sex, hatchery, or origin, as our sample size was not large enough to detect these differences, if they exist. While ShapeR is certainly useful, it is still limited in comparison to the 3D Slicer by its processing speed and the limitations inherent to 2D analyses.

The automated 3D μ CT scanner was an order of magnitude faster at measuring the set of 35 otolith pairs compared to either of the other two techniques (manual 2D and automated 2D). While both the ShapeR and the μ CT scanner can measure otoliths while the researcher works on other tasks, it is still preferable to have a method that produces results faster. ShapeR produces output errors frequently enough that fisheries scientists are almost guaranteed to encounter them in any sample set run. In this study for example, four of the 70 photos had to be rerun in ShapeR due to output errors. As a consequence, ShapeR data will almost always require some reanalysis, further adding analysis time. There appears to have been a single measurement error in the 3D measurements, but it did not impact any of the findings in the study.

In the sample set used in the study, there was a significant difference in the density of otoliths, with coho from Quinsam hatchery having otoliths that were roughly 8% denser on average than fish from the other two hatcheries. In contrast, the 2D analysis comparing superficial density had more variability in terms of the observations around the means as the z axis was not captured and thus showed no differences across hatcheries. While it is not surprising that there were no differences between hatcheries found in either the manual 2D or automated 2D methods, it is very surprising that such a clear difference between hatchery populations was noted by the 3D method with such few samples. Similar conclusions have been noted before when comparing the results of 2D and 3D morphometrics; if there is relevant z axis information lost in the conversion to 2D, then 3D methods are more accurate in representing the overall structure (Meyer et al. 2009; Buser et al. 2018). The 2D conversion of 3D data will essentially mask the differences among populations if relevant z axis information is not accurately represented.

When comparing data quality and quantity, 3D otolith morphometrics allow fisheries scientists to collect more data from their otoliths, such as otolith volume and density (as seen in this study and Radford et al. 2021) and whole otolith contour analyses (as seen in Marti-Puig et al. 2016). Both methods may have been

able to approach a similar conclusion, that there are differences in otolith densities between coho hatchery populations, but to have equivalent statistical power, we would need to process otoliths from roughly 30 times more fish in the 2D analysis. This does not exactly mean that the 3D method will produce significant results in 3–4 fish every time, but that where there are differences in populations, the 3D method will likely require far fewer samples than any 2D method attempting to reduce the z axis to produce similar data. The lack of statistical power compounds with the extra time 2D manual and 2D automatic methods take, and so processing this many more otoliths would take over 100 times as long. These results are based on our sample set; it is possible that these results will vary based on species and the differences among populations of the species. Regardless, if our sample set is representative, and if there is a significant difference that involves z axis information, automated 3D methods are clearly better. Even if there is not a significant difference that involves z axis information in another dataset, automated 3D methods are still better than rival 2D methods as processing time is about 4.5 times faster. This method should be applicable to the vast majority of fish species as the general form of otoliths is well conserved. There are some fish species, such as the California flashlightfish (*Protomyctophum crockeri*), that have more squat otoliths, so both ShapeR and 3D Slicer would misinterpret the width as the length since is the longest dimension. However, these issues could be easily accounted for with some diligence on the part of the researcher.

The difference in densities across these hatcheries is interesting as otolith density plays a role in how fish hear (Oxman et al. 2007). These otoliths all looked aragonitic under a dissecting microscope, yet none of them were near the commonly cited value of $2.93 \text{ g}\cdot\text{cm}^{-3}$, and in fact all but one population had average otolith densities lower than the reported value for vateritic otoliths, $2.65 \text{ g}\cdot\text{cm}^{-3}$ (Campana and Thorrold 2001). There are a couple of possible explanations. It may be that since organic matter is incorporated into the otolith at roughly 0.2%–10% of the otolith by mass (Degens et al. 1969), this may vary across the different populations, which could cause a difference in density. While the regulation of otolith increment formation is not well understood (Thomas and Swearer 2019), it is possible that there is a difference in a regulatory pathway that causes differences in increment formation between populations that manifests as differences in otolith density at the macroscopic level. Another possibility is that there may be differences in raising conditions that may lead to some of these populations experiencing increased CO_2 levels, thus experiencing a more acidic environment. This has been found to impact the volume and mass of fish otoliths (Bignami et al. 2013). However, there was no difference in otolith density between hatchery and wild fish within each hatchery, which may indicate that there is some baseline genetic basis for the difference, as hatcheries tend to use wild fish as part of their broodstock and hatchery fish do interbreed with the wild fish outside of the hatchery. Whatever the case may be, this result has implications for the hearing and behavior of these coho, as well as the use of methodologies that assume generalizations about otolith composition, such as Laser Ablation Inductively Coupled Plasma Mass Spectrometry (Brophy et al. 2003). We would not have found this result as easily, if at all, without the use of a 3D analysis.

The future of otolith morphometrics is in high-throughput, automated, 3D, quantitative morphometric analyses. Other advancements in the field could come by machine learning to automate the collection of landmarks, thus allowing for geometric morphometric analyses. Otoliths contain relevant z axis information, therefore reducing an analysis to two dimensions loses biologically relevant data. Using the method(s) put forward here will result in more and better data every time. Fisheries scientists would have the ability to run hundreds of otoliths a day, answer a wider range

of questions, and free themselves from repetitive methods that can be accomplished by machines. While the startup cost of μ CT scanning equipment is great, there are facilities that are able to run CT scans at very low costs. Throughout this study, the use of automated 3D μ CT scanners produced more data, with more statistical power, faster and more efficiently than alternative methods; other methods for otolith morphometrics may simply be outdated.

Competing interests

The authors declare there are no competing interests.

Contributors' statement

MJQ: substantial contributions to the conception and design of the work, collection of all 2D data, data analysis and interpretation, drafting and revision of the manuscript, agreement to be accountable for all aspects of the work, and final approval of the version to be published. APS: substantial contributions to the conception and design of the work, collection of all 3D data, revision of the manuscript, and final approval of the version to be published. FJ: substantial contributions to the conception and design of the work, principal investigator, revision of the manuscript, and final approval of the version to be published.

Funding statement

Funding for this research was provided by NSERC, the Pacific Salmon Foundation, CFI/BCKDF and the Liber Ero Foundation.

Acknowledgements

The Watershed Enhancement Managers, Aaron Burgoyne, Edward Walls, and Jeremy Mothus are acknowledged here for access to each hatchery. The Whiteley Center at the Friday Harbor Labs is thanked for the time to “hatch” these ideas.

References

- Adams, D.C., Rohlf, F.J., and Slice, D.E. 2004. Geometric morphometrics: ten years of progress following the ‘revolution’. *Ital. J. Zool.* **71**: 5–16. doi:10.1080/11250000409356545.
- Afanasyev, P.K., Orlov, A.M., and Rolsky, A.Y. 2017. Otolith shape analysis as a tool for species identification and studying the population structure of different fish species. *Biol. Bull. Russ. Acad. Sci.* **44**: 952–959. doi:10.1134/S1062359017080027.
- Bignami, S., Enochs, I.C., Manzello, D.P., Sponaugle, S., and Cowen, R.K. 2013. Ocean acidification alters the otoliths of a pantropical fish species with implications for sensory function. *Proc. Natl. Acad. Sci. U.S.A.* **110**(18): 7366–7370. doi:10.1073/pnas.1301365110. PMID:23589887.
- Brophy, D., Danilowicz, B.S., and Jeffries, T.E. 2003. The detection of elements in larval otoliths from Atlantic herring using laser ablation ICP-MS. *J. Fish Biol.* **63**: 990–1007. doi:10.1046/j.1095-8649.2003.00223.x.
- Buser, T.J., Sidlauskas, B.L., and Summers, A.P. 2018. 2D or not 2D? Testing the utility of 2D vs. 3D landmark data in geometric morphometrics of the sculpin subfamily Oligocottinae (Pisces; Cottoidea). *Anat. Rec.* **301**(5): 806–818. doi:10.1002/ar.23752.
- Buser, T.J., Boyd, O.F., Cortés, Á., Donatelli, C.M., Kolmann, M.A., Luparell, J.L., et al. 2020. The natural historian's guide to the CT galaxy: step-by-step instructions for preparing and analyzing computed tomographic (CT) data using cross-platform, open access software. *Integr. Org. Biol.* **2**(1): obaa009. doi:10.1093/iob/obaa009. PMID:33791553.
- Campana, S.E., and Casselman, J. 1993. Stock discrimination using otolith shape analysis. *Can. J. Fish. Aquat. Sci.* **50**(5): 1062–1083. doi:10.1139/f93-123.
- Campana, S.E., and Thorrold, S.R. 2001. Otoliths, increments, and elements: keys to a comprehensive understanding of fish populations? *Can. J. Fish. Aquat. Sci.* **58**(1): 30–38. doi:10.1139/f00-177.
- Cardini, A. 2014. Missing the third dimension in geometric morphometrics: how to assess if 2D images really are a good proxy for 3D structures? *Hystrix*, **25**: 73–81. doi:10.4404/hystrix-25.2-10993.
- Conover, D.O. 1990. The relation between capacity for growth and length of growing season: evidence for and implications of countergradient variation. *Trans. Am. Fish. Soc.* **119**: 416–430. doi:10.1577/1548-8659(1990)119<0416:TRBCFG>2.3.CO;2.
- Degens, E.T., Deuser, W.G., and Haedrich, R.L. 1969. Molecular structure and composition of fish otoliths. *Mar. Biol.* **2**: 105–113. doi:10.1007/BF00347005.
- Geffen, A. 1982. Otolith ring deposition in relation to growth rate in herring (*Clupea harengus*) and turbot (*Scophthalmus maximus*) larvae. *Mar. Biol.* **71**: 317–326. doi:10.1007/BF00397048.
- Green, P., and MacLeod, C.J. 2016. SIMR: an R package for power analysis of generalized linear mixed models by simulation. *Methods Ecol. Evol.* **7**: 493–498. doi:10.1111/2041-210X.12504.
- Hipsley, C.A., Aguilar, R., Black, J.R., and Hocknull, S.A. 2020. High-throughput micro CT scanning of small specimens: preparation, packing, parameters and post-processing. *Sci. Rep.* **10**: 13863. doi:10.1038/s41598-020-70970-7. PMID:32807929.
- Hüssy, K., Mosegaard, H., Albertsen, C.M., Nielsen, E.E., Hemmer-Hansen, J., and Eero, M. 2016. Evaluation of otolith shape as a tool for stock discrimination in marine fishes using Baltic Sea cod as a case study. *Fish. Res.* **174**: 210–218. doi:10.1016/j.fishres.2015.10.010.
- Libungan, L.A., and Pálsson, S. 2015. ShapeR: an R package to study otolith shape variation among fish populations. *PLoS ONE*, **10**(3): e0121102. doi:10.1371/journal.pone.0121102. PMID:25803855.
- Marti-Puig, P., Danés, J., Manjabacas, A., and Lombarte, A. 2016. New parameterisation method for three-dimensional otolith surface images. *Mar. Freshw. Res.* **67**: 1059–1071. doi:10.1071/MF15069.
- Meyer, M.G., Fauver, M., Rahn, J.R., Neumann, T., Patten, F.W., Seibel, E.J., and Nelson, A.C. 2009. Automated cell analysis in 2D and 3D: a comparative study. *Pattern Recognit.* **42**(1): 141–146. doi:10.1016/j.patcog.2008.06.018.
- Mosegaard, H., Svedäng, H., and Taberman, K. 1988. Uncoupling of somatic and otolith growth rates in Arctic char (*Salvelinus alpinus*) as an effect of differences in temperature response. *Can. J. Fish. Aquat. Sci.* **45**(9): 1514–1524. doi:10.1139/f88-180.
- Oxman, D.S., Barnett-Johnson, R., Smith, M.E., Coffin, A., Miller, D.L., Josephson, R., and Popper, A.N. 2007. The effect of vaterite deposition on sound reception, otolith morphology, and inner ear sensory epithelia in hatchery-reared Chinook salmon (*Oncorhynchus tshawytscha*). *Can. J. Fish. Aquat. Sci.* **64**(11): 1469–1478. doi:10.1139/f07-106.
- Pannella, G. 1971. Fish otoliths: daily growth layers and periodical patterns. *Science*, **173**: 1124–1127. doi:10.1126/science.173.4002.1124. PMID:5098955.
- Phillips, J.B. 1948. Comparison of calculated fish lengths based on scales from different body areas of the sardine, *Sardinops caerulea*. *Copeia*, **1948**(2): 99–106. doi:10.2307/1438411.
- Popper, A.N., and Lu, Z. 2000. Structure–function relationships in fish otolith organs. *Fish. Res.* **46**: 15–25. doi:10.1016/S0165-7836(00)00129-6.
- Radford, C.A., Collins, S.P., Munday, P.L., and Parsons, D. 2021. Ocean acidification effects on fish hearing. *Proc. R Soc. B Biol. Sci.* **288**: 20202754. doi:10.1098/rspb.2020.2754. PMID:33653144.
- R Core Team. 2020. R: A language and environment for statistical computing. R Foundation for Statistical Computing, Vienna, Austria. Available from <https://www.R-project.org/>.
- Rohlf, F.J., and Marcus, L.F. 1993. A revolution morphometrics. *Trends Ecol. Evol.* **8**: 129–132. doi:10.1016/0169-5347(93)90024-J. PMID:21236128.
- RStudio Team. 2015. RStudio: Integrated Development for R. RStudio, Inc., Boston, Mass. Available from <https://www.rstudio.com>.
- Schulz-Mirbach, T., Heß, M., and Plath, M. 2011. Inner ear morphology in the Atlantic molly *Poecilia mexicana* — first detailed microanatomical study of the inner ear of a cyprinodontiform species. *PLoS ONE*, **6**(11): e27734. doi:10.1371/journal.pone.0027734. PMID:22110746.
- Sokal, R.R. 1965. Statistical methods in systematics. *Biol. Rev.* **40**(3): 337–389. doi:10.1111/j.1469-185X.1965.tb00806.x. PMID:14340912.
- Song, J., Zhao, B., Liu, J., Cao, L., and Dou, S. 2019. Comparative study of otolith and sulcus morphology for stock discrimination of yellow drum along the Chinese coast. *J. Ocean. Limnol.* **37**: 1430–1439. doi:10.1007/s00343-019-8056-6.
- Thomas, O.R., and Swearer, S.E. 2019. Otolith biochemistry — a review. *Rev. Fish. Sci. Aquacult.* **27**: 458–489. doi:10.1080/23308249.2019.1627285.
- Thompson, D.W. 1917. On growth and form. Cambridge University Press, Cambridge, UK.
- Tracey, S.R., Lyle, J.M., and Duhamel, G. 2006. Application of elliptical Fourier analysis of otolith form as a tool for stock identification. *Fish. Res.* **77**: 138–147. doi:10.1016/j.fishres.2005.10.013.
- Waessle, J.A., Lasta, C.A., and Favero, M. 2003. Otolith morphology and body size relationships for juvenile Sciaenidae in the Río de la Plata estuary (35–36° S). *Sci. Mar.* **67**(2): 233–240. doi:10.3989/scimar.2003.67n2233.
- Wickham, H. 2016. ggplot2: Elegant graphics for data analysis. Springer-Verlag, New York.